Int J Appl Earth Obs Geoinformation 80 (2019) 230–239

Contents lists available at ScienceDirect

Int J Appl Earth Obs Geoinformation

journal homepage: www.elsevier.com/locate/jag

An approach for heavy metal pollution detected from spatio-temporal stability of stress in rice using satellite images

Meiling Liu[a,*], Andrew K. Skidmore[b,c], Tiejun Wang[b], Xiangnan Liu[a], Ling Wu[a], Lingwen Tian[a]

[a] School of Information Engineering, China University of Geosciences, Beijing 100083, China
[b] Faculty of Geo-Information Science and Earth Observation (ITC), University of Twente, P.O. Box 217, 7500 AE Enschede, the Netherlands
[c] Department of Environmental Science, Macquarie University, NSW 2109, Australia

ARTICLE INFO

Keywords:
Spatio-temporal stability
Stable stress
Satellite imagery
Wavelet transform

ABSTRACT

Stable stressors on crops (e.g., salts, heavy metals), which are characterized by stable spatial patterns over time, are harmful to agricultural production and food security. Satellite data provide temporally and spatially continuous synoptic observations of stable stress on crops. This study presents a method for identifying rice under stable stress (i.e., Cd stress) and exploring its spatio-temporal characteristics indicators. The study area is a major rice growing region located in Hunan Province, China. Moderate-resolution imaging spectroradiometer (MODIS) and Landsat images from 2008–2017 as well as in *situ* measurements were collected. The coupling of a leaf canopy radiative transfer model with the World Food Study Model (WOFOST) via a wavelet transform isolated the effects of Cd stress from other abrupt stressors. An area wavelet transform stress signal (AWTS), based on a time-series Enhanced Vegetation Index (EVI), was used to detect rice under Cd stress, and its spatio-temporal variation metrics explored. The results indicate that spatial variation coefficients (SV_C) of AWTS in the range of 0–1 ha d a coverage area greater than 70% in each experimental region, regardless of the year. Over ten years, the temporal variation coefficients (TV_C) of AWTS in the range of 0–1 occurred frequently (more than 60% of the time). In addition, the Pearson correlation coefficient of AWTS over two consecutive years was usually greater than 0.5. We conclude that a combination of multi-year satellite-derived vegetation index data with a physical model simulation is an effective and novel method for detecting crops under environmental stress. A wavelet transform proved promising in differentiating between the effects of stable stress and abrupt stress on rice and may offer a way forward for diagnosing crop stress at continental and global scales.

1. Introduction

Crop stress is defined as any environmental factor that is potentially unfavorable to crops' metabolism, growth, or development (Levitt, 1980; Lichtenthaler, 1998). Environmental stressors are increasingly affecting crop production around the world. It has been reported that crop production is limited by a suite of environmental stressors resulting in 30%–60% yield losses globally each year (Dhlamini et al., 2005). Crop stressors are typically classified as being either abrupt or stable. Abrupt stressors (e.g., drought, pests/diseases, and mismanagement) are transient, often varying intra-annually (Scudiero et al., 2014). Conversely, stable stressors (e.g., salts, heavy metals) are defined herein as stressors that are relatively stable in space over long time scales (within a decade) and persistent throughout all crop growth stages (Liu et al., 2016a,b,c, 2018a,b; Tian et al., 2017). Heavy metals, which are influenced by natural and anthropogenic factors, including parent materials, land use, and application of pesticides and fertilizers, are extremely persistent in the environment; they are non-biodegradable and non-thermo-degradable and thus readily accumulate to toxic levels (Nagajyoti et al., 2010). Heavy metal stress, which occurs on a regional scale, is a major cause of crop loss. Soil to crop transfer is one of the key components of human exposure to heavy metals through the food chain and poses serious human health risks (Srivastava et al., 2017). Quantifying stress in crops caused by heavy metals is critical for agricultural production and food safety.

Stress-induced damage in crops has been detected using reflectance spectra (Ren et al., 2009; Liu et al., 2010, 2011a, 2011b; Wang et al., 2012, 2018). Reflectance spectra or vegetation indices of crops do indicate variation throughout all crop growth stages, with heavy metal stress for a crop being persistent in a specific region and thus changes the crops' growth trajectory (Wu et al., 2013; Tian et al., 2017). In other words, dynamic changes in vegetation indices or physiological

* Corresponding author.
E-mail address: liuml@cugb.edu.cn (M. Liu).

https://doi.org/10.1016/j.jag.2019.04.012
Received 19 January 2019; Received in revised form 9 April 2019; Accepted 12 April 2019
Available online 04 May 2019

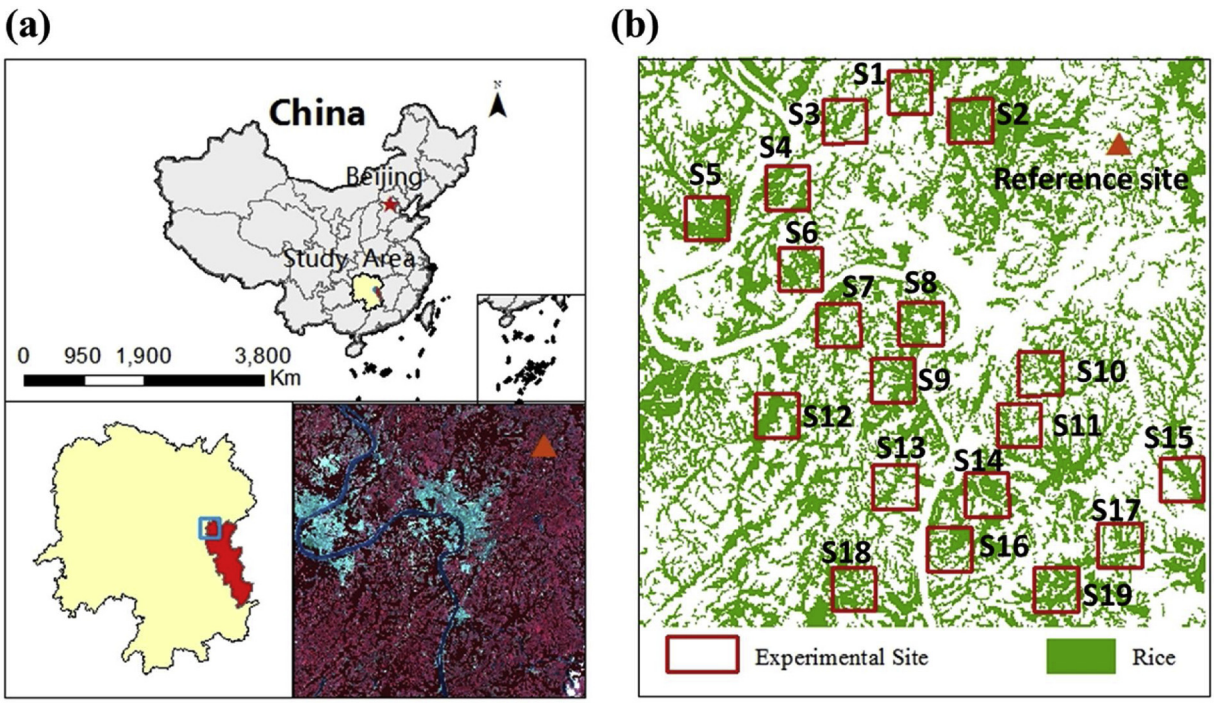

Fig. 1. Description of the study area: (a) Location of the study area in Hunan Province, China; (b) the distribution of 19 experimental sites.

parameters can reflect the growth trajectory of crops under various stress conditions. For example, Tian et al. (2017) suggested that crop tissues or variation in physiological parameters, such as leaf area index (LAI) values simulated using the Enhanced World Food Studies (WOFOST) model, and then combined with remotely sensed data collected during all the growth stages, could be used to detect heavy metal stress in rice. However, healthy rice and heavy-metal-stress-induced rice were not compared by Tian et al. (2017). One particular method that holds considerable promise for assessing crop growth states in unstressed environmental conditions is the use of a crop growth model, such as the WOFOST model (Jin et al., 2015; Liu et al., 2016a,b,c). This crop growth model can be used to predict the potential growth, development, and yield of crops on a continuous time scale when a set of relevant biological and environment parameters are provided (Montieth, 1996). Vegetation indices of healthy rice over all the growth stages have been derived, when the crop growth model has been coupled to the PROSPECT + SAIL canopy radiative transfer model (Jacquemoud et al., 2009; Wu et al., 2013). The accurate calculation of stress signals in crops is made possible by combining simulated data with remotely sensed data (Whitney et al., 2018).

However, in real agricultural ecosystems, two different types of stressors, abrupt and stable, act simultaneously on crops, resulting in the frequent combination of the effects of heavy metals, pests, and diseases on the crops' growth periods. The challenge thus arises of how to isolate the effects of stable stressors from abrupt stressors. Multi-temporal analysis of vegetation indices can be used to differentiate between stable stressors and abrupt stressors, since vegetation indices' time series are characterized by patterns such as a crop's intrinsic growth trend and stationary and localized abrupt changes or discontinuities resulting from continuous and disturbance events respectively (de Beurs and Henebry, 2005; Campos and Bella, 2012; Scudiero et al., 2014; Tian et al., 2017). Application of a wavelet transform (WT) is a well-known and promising approach to analyzing non-stationary and stationary signal variations. For example, the relationship between variation in vegetation indices and climate anomalies have been explored using this approach (Li and Kafatos, 2000; Wang et al., 2001; Tateishi and Ebata, 2004; Erasmi et al., 2009). WTs have been used to capture and describe non-stationary and stationary variations in vegetation indices (Martinez and Amparo Gilabert, 2009 Li and Kafatos, 2000; Piao et al., 2012). We therefore concluded that it may be feasible to employ a WT to distinguish between rice under stable stress and rice under abrupt stress.

Heavy metal stress is considered to be fairly stable over long periods of time (e.g., a decade). To reveal the stable characteristics of rice under heavy metal stress, a long time frame and large spatial scale, which can be provided by a long time series of satellite images (e.g., MODIS and Landsat remotely sensed data), were considered in this research. In general, compared with MODIS alone, combined high temporal and spatial resolution can make it easy to discriminate farm land from non-agricultural features and thus monitor crop growing processes (Gao et al., 2006). Satellite images can be employed to obtain the EVI of rice growing on a large scale over all the growth stages of a plant over multiple years. Multi-year data make it possible to identify similarities in the stable stress signal over a long time period such as a decade. In addition, complete growth stage data make it possible to detect the dynamic and continuous processes of heavy metal accumulation in crops as they affect the stable stress signal, which reflects the degrees of heavy metal stress on crops at different stages and explains the soil's heavy metal pollution conditions.

Recently, researchers have mapped salinity over semi-arid farmland using multiple-year time series of vegetation indices derived from MODIS and Landsat (Lobell et al., 2007, 2010; Scudiero et al., 2014, 2015; Whitney et al., 2018; Paliwal et al., 2018). These studies focused on establishing the relationships between multi-year maxima, average values of vegetation indices, and ground-truth soil salinity. Previous attempts to use satellite imagery to assess soil salinity were unsuccessful in isolating the effects of stable salinity stress on vegetative growth from the effects of other abrupt factors. The objectives of this study were to (i) extract the heavy metal stress signal from the data by isolating the effects of heavy metal stress on rice from the effects of other abrupt stressors and (ii) exploring the spatio-temporal characteristics indicators for heavy metal stress on rice.

2. Study area and data

2.1. Study area

The study area is a heavy-metal-contaminated area (2025 km^2) located in Hunan Province, China (centered at Lat. 27°48′9″ N, Lon. 113°6′24″ E) (Fig. 1). This area is characterized by a subtropical monsoon climate with a mean annual temperature of approximately 16–18 °C and a mean annual rainfall of approximately 1500 mm. This area is a typical red soil hilly landform, and has dense rive network and developed agricultural irrigation system. About 35% of the land was used for agricultural farming, 52% of the land was occupied by forests. And the rest occupied by residential settlements, factories, river and roads. The predominant soil type is red soil with sufficient organic matter (2–3%). Rice is the dominant crop in this region, for the single-rice cropping region in Hunan Province, the rice is often transplanted in early June and harvested in late September.

To analyze the spatio-temporal characteristic of the rice under heavy metal stress, 19 experimental sites were selected, based on the spatially widespread and continuous rice distribution. All experimental sites were planted with rice over ten years. Thus, land use of experimental sites is hardly changed. The experimental sites were designated S1, S2, S3, etc., through S19 (Fig. 1). Reference squares covering 120 × 120 Landsat pixels (12.96 km^2) were delineated to create a rice paddy mask. The spatial distribution of paddies with a spatial resolution of 30 m was obtained from the Global Agriculture Maps (https://web.croplands.org). The pixel numbers corresponding entirely to the rice paddies measured in each experiment are shown in Table S1. This is an important industrial zone, as well as an agricultural zone, and the agricultural land being impacted by industrial activities. Previous studies have shown that Cd is the predominant pollutant in paddy soils that are watered from the Xiang Jiang River, which contains industrial wastewater discharge (Lei et al., 2015; Chen et al., 2016). Heavy metal ions, especially Cd, in the Xiang Jiang River have been found to be much higher than those in the soil trace element background for Hunan Province (Liu et al., 2017). The soil Cd concentrations in the experimental sites range from 0.9 to 9 $mg.kg^{-1}$ (the threshold value soil of Level II Soil Environmental Quality Standards in China is 0.3 $mg\,kg^{-1}$). It should be noted that differences in the soil Cd concentration among the experimental sites were not considered in the analysis because the spatio-temporal characteristics of rice under heavy metal stress were analyzed with respect to each individual experimental region. To obtain the test data for the EVI simulation, one control site in the study area (designated the “Reference site”) was identified. This site has been unstressed by Cd; has had rice growing in the field from 2014 to 2016; has been cultivated on an experimental farm; and has been supplied with abundant fertilizers, manure, and irrigation water to avoid other environmental factors causing unwanted stress.

2.2. Remote sensing data

The Landsat-8 Operational Land Imager (OLI), Landsat-7 Enhanced Thematic Mapper Plus (ETM+), and MOD09A1 (MODIS surface reflectance products) from 2008–2017 were used in this study. To improve the quality of the data fusion, all of the data available for the study area between late April and late October, which is a longer period than the rice growing season, were selected. The MOD09A1 product is eight-day composite surface reflectance data with a spatial resolution of 500 m (https://ladsweb.modaps.eosdis.nasa.gov). The Landsat series data, which were downloaded from the USGS Earth Explorer website (http://earthexplorer.usgs.gov), have a spatial resolution of 30 m and a temporal resolution of 16 d. High-quality Landsat images (with cloud cover less than 35%) of the study area were selected. A total of 250 images were selected: 70 Landsat images and 180 MODIS images (Fig. S1). The MOD09A1 product provides bands 1–7, while Landsat-8 OLI and Landsat-7 ETM + include bands 1–8 and bands 1–9. Blue, green, red, and near-infrared in all images were used. Further information is provided in Table S2.

2.3. In situ measured data

We carried out investigations and data collection during typical rice growth stages from 2014 – 2016. Topsoil samples were collected at depths in the range of 0–20 cm. The metal Cd concentration in the soil was analyzed by the Chinese Academy of Agricultural Sciences, Beijing, China. Soil samples were also analyzed for heavy metal extractable with diethylenetriaminepentaacetic acid using the method proposed by Lindsay and Norvell (1978) and the AAS to determine Cd concentrations. The LAI of the study area was determined nondestructively using a botanical canopy analyzer (AccuPAR model LP-80, METER Group, Inc., USA) at five random positions in each sample plot. Leaf chlorophyll was determined using a SPAD-502 portable chlorophyll meter (Minolta Corporation, Ramsey, NJ, USA). All spectral measurements were taken under cloudless or near-cloudless conditions between 10:00 and 14:00 using an ASD FieldSpec Pro spectrometer (Analytical Spectral Devices, Boulder, CO, USA). The spectrometer was fitted with 10°-field-of-view fiber optics and operated in the 350–2500 nm spectral region at sampling intervals of 2 nm.

The meteorological data used in this study included daily maximum and minimum air temperatures and the actual daily hours of sunshine (Table S3). The data for 2008–2017 were downloaded from the China Meteorological Administration (http://www.cma.gov.cn/). These data were transformed into solar radiation as a climatic input parameter for the enhanced WOFOST model (Liu et al., 2004; Van Laake and Sanchez-Azofeifa, 2005). Phenological information, including the transplanting date (i.e., the first ten-day period of June), anthesis date (i.e., the first ten-day period of August) and harvesting data of rice (i.e., the last ten-day period of September) for the study area was obtained from China Agriculture and Affairs (http://www.zzys.moa.gov.cn).

3. Methods

An important methodological step is establishing a clear conceptual framework for defining the stress signal, defined herein as stress-induced spectral variation that represents the difference between the vegetation index of healthy rice and the vegetation index of stressed rice. The procedure for the calculation and characterization of the stress signal can be summarized as follows (see Fig. 2). (i) The vegetation index of rice growing in a real agricultural ecosystem (i.e., stressed rice) was calculated by blending selected bands of the Landsat and MODIS images (Fig. 2a). (ii) The vegetation index of healthy rice was simulated using a theoretical model (Fig. 2b). (iii) The stress signal was evaluated by application of a wavelet transform to isolate stable stress from abrupt stress (Fig. 2c). (iv) Key parameters of the spatio-temporal variations of the stress signal were selected (Fig. 2d).

3.1. Reconstruction of VI time series

To generate time series data with a high spatial and temporal resolution, we applied cloud and cloud shadow masks generated from the Quality Flag in the MOD09A1 product as well as data preprocessing, including radiance calibration, atmospheric correction, image clipping, and resampling. The Enhanced Spatial and Temporal Adaptive Reflectance Fusion Model (ESTARFM) was used to obtain a time series of the 8-d surface reflectance product (30 m) by blending the selected bands of Landsat and MODIS images (Zhu et al., 2010; Gao et al., 2015). The ESTARFM algorithm uses two pairs of Landsat–MODIS images (i.e., dates t_1 and t_3) and one MODIS image (date t_2) to predict a Landsat-like image at date t_2. In this study, a total of 115 synthetic fine-resolution images that covered the rice growing seasons from 2008–2017 were created.

In this study, EVI was used to evaluate the process of paddy growth

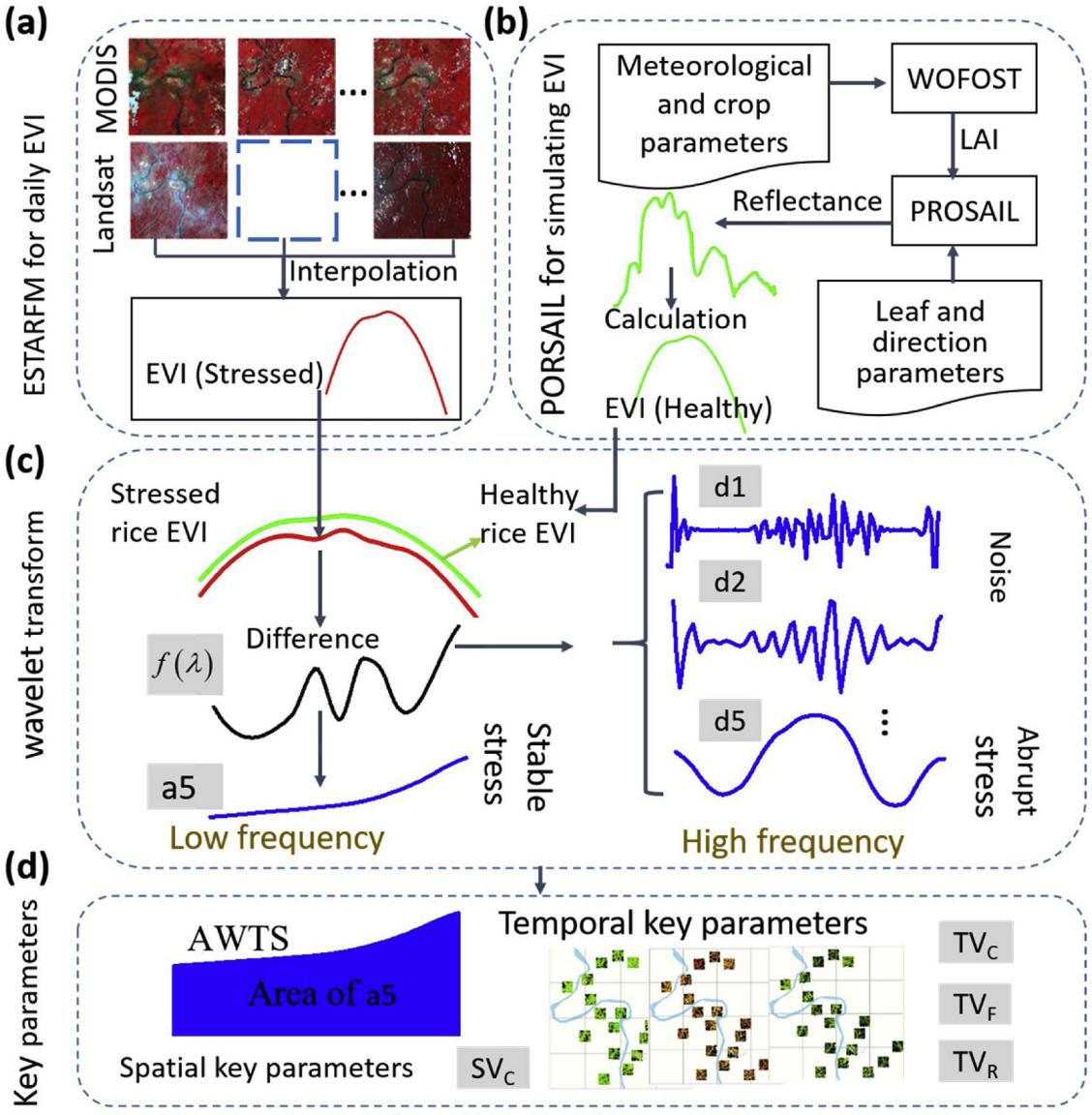

Fig. 2. Flow chart for extraction and analysis of rice under stable stress.

adequately over a wide dynamic range, due to the fact that EVI is more practical than NDVI for rice growing in high humidity and in the rainy season (Huete et al., 2002; Sakamoto et al., 2005). It was necessary to reconstruct the time-series EVI data before application because of the considerable noise present. The EVI time series were fitted using double-logistic filtering (Jonsson and Eklundh, 2002, 2004; Bradley et al., 2007; Hird and McDermid, 2009; Liu et al., 2018a, b).

3.2. Radiation transfer model coupled with the WOFOST model

The WOFOST and PROSPECT models were used to simulate the VI of healthy rice. The PROSAIL model is a coupled model of the PROSPECT leaf optical properties model and the 4SAIL canopy bi-directional reflectance model, which is widely used to calculate canopy reflectance (Feret et al., 2008; Jacquemoud et al., 2009); in this study, the PROSAIL model was used to simulate the canopy reflectance of healthy rice. Details of the input parameters used with the PROSAIL model are shown in Table S4. The three main types of parameters are as follows: (1) leaf parameters, namely the leaf mesophyll structure parameter (Ns), leaf a and b content (Cab), leaf equivalent water thickness (Cw), leaf dry matter content (Cm), leaf brown pigment content (Cbr), and carotenoid content (Car); (2) canopy parameters, namely the leaf area index (LAI), average leaf angle (ALA), hotspot parameters (hotspot), and soil brightness parameters (Psoil); and (3) illumination parameters, namely, the fraction of diffused incoming solar radiation (SKYL), sun zenith angle (SZA), sensor zenith angles (VZA), and azimuth angle between the sun and the sensor (RAA).

Previous studies have demonstrated that the value of physiological parameters, such as the chlorophyll content, water content, and LAI, often change when crops are exposed to environmental stressors (Levitt, 1980; Ren et al., 2009; Liu et al., 2010) and that this triggers variation in the crops' reflectance spectra. Wu et al. (2012) conducted a sensitivity analysis and found that variation in the chlorophyll content, water content, and LAI resulted in variation in the reflectance of the visible light, middle-infrared, and whole-region bands between 350 nm and 2500 nm, respectively. EVI is calculated over the NIR band, red band, and blue band. In other words, EVI is mostly affected by the chlorophyll content and LAI, rather than the water content. Our field investigation found that the chlorophyll content in rice is closely correlated to the rice LAI. Based on the chlorophyll content and rice LAI data collected from 2014 to 2016 (Fig. S2), the chlorophyll content was calculated from the LAI simulation using the following equation:

$$y = -3.747x^2 + 44.450x - 92.576 \quad (1)$$

where y is the chlorophyll content and x is the LAI. The coefficient of determination (R^2) between the measured chlorophyll content and the predicated chlorophyll content was 0.701.

Based on these analysis results, the primary emphasis was on deriving LAI and then calculating the EVI (Wu et al., 2012, 2013). The LAI was derived from the WOFOST model. The WOFOST model is a dynamic and interpretative model that simulates the LAI growth of a crop at a daily time step under specific soil and climate conditions. This simulation can be implemented at the potential productivity level on the basis of the main factors that limit crop growth, such as the solar radiation and temperature. The input parameters of the WOFOST model were set on the basis of values reported in the literature of this study area (Jin et al., 2015; Huang et al., 2016; Liu et al., 2016a, b, c; Zhou et al., 2017). The primary parameter values used are shown in Table S5. The values of other parameters in the PROSAIL model were derived from LOPEX (Ceccato et al., 2001; Hosgood et al., 1994; Zhou et al., 2017) and remote sensing data (Table S4). It should be noted that the growth of healthy rice in a given year at any site within this area is expected to be the same because they experienced the same meteorological conditions. Thus, the single growth curve of simulated EVI by WOFOST and PROSAIL model represents healthy rice at 19 experimental sites. To confirm the credibility of the EVI simulation, the simulated EVI was tested against our field data collected from 2014 – 2016.

3.3. Obtaining a stable stress signal (AWTS) using a wavelet transform

The wavelet transform (WT) has excellent time and frequency properties by decomposing the wavelet low-frequency component (a_j) and high-frequency components (d_j) (denoted by subscript numbers). The equation is as follows:

$$f(\lambda) = a_j(\lambda) + \sum_{i=1}^{j} d_i(\lambda) \tag{2}$$

Here, $f(\lambda)$ is original signal, a_j represents the high-scale, low-frequency components of a signal and is associated with averages over scales, and it can capture the stationary level of the original signal (Percival and Walden, 2000). d_j represent the low-scale, high-frequency components, and it is well suited to detecting transient changes and hence is associated with fluctuations and abnormal variations on a scale.

Based on the above analysis, we assumed that the frequency of noise components and abrupt stress in rice are included in the high-frequency components of the rice stress signal EVI and that the stable stress of rice is related to the low-frequency component of the rice stress signal. We used a routine written in MATLAB (the Mathworks, Inc., Natick, Massachusetts, USA) to apply discrete wavelet decompositions to each of the original stress signal with the Daubechies wavelet ("db5") (Liu et al., 2011a,b). Different decomposition scales for the db5 wavelet have been tested, and the results have shown that scale 32 ($= 2^5$) is effective in detecting heavy metal stress information in a satisfactory way by eliminating the abrupt change and noise in time-series VI data around the planting and harvesting seasons of rice (Liu et al., 2011a,b; Sakamoto et al., 2005). In this way, the original stress signal was decomposed into a low-frequency component (a5) and high-frequency components (d1–d5).

In this study, a new proposed index, namely an area wavelet transform stress signal (AWTS) was calculated. Three steps were taken to achieve a stable stress signal (AWTS) (Fig. 2c and d):

(1) subtracting the stressed rice EVI (i.e., the observed EVIs) by the healthy rice EVI (i.e., simulated EVIs) as the original stress signal (Fig. 2c).

(2) extracting a5 by using wavelet transform at the fifth decomposition level, as mentioned above (Fig. 2c).

(3) calculating the area of (a5) from DOY152 (the 152nd day of the year) to DOY 262 over the entire growth stage (denoted AWTS) (Fig. 2d).

3.4. Constructing key parameters for spatio-temporal characteristics

To validate the spatio-temporal stability of AWTS for monitoring Cd stress in rice in each experimental region over ten years (i.e., 10-yr), four categories of parameters were selected to study the spatial and temporal variations of AWTS. The first category of parameters related to the spatial variation of AWTS. The coefficients of spatial variation (SV_C) were defined as follows (Fig. S3(a)).

$$SV_C = \frac{|SV_C j,\ i - \overline{SV_C}|}{\delta_{j,i}} \tag{3}$$

where $SV_C j$, i, $\overline{SV_C}$, and $\delta_{j,i}$ are the i^{th}-pixel AWTS value in the j^{th} experimental region (j = 1–19), the area-averaged mean value, and the standard deviation along a given AWTS in the j^{th} experimental region, respectively. SV_C is divided into three groups, namely $0 < SV_C \leq 1$, $1 < SV_C \leq 2$, and $SV_C > 2$. The lowerSV_C is, the greater the homogeneity of $SV_C$is. When crops are stressed by stable stressors, SV_Chas a lower value because the AWTS changes uniformly within this area. It should be noted that the values of 1 and 2 represent 99% and 95% confidence levels, which are often considered effective threshold values of "stable status" versus "abnormal status."

Similarly, the second category of parameters are related to temporal variation features of AWTS and are defined as follows.

(1) TV_C, the coefficients of temporal variation for AWTS TV_C, formulated simply as follows (Fig. S3(b)):

$$TV_C = \frac{|TV_{Cm,i} - \overline{TV_C}|}{\delta_{m,i}} \tag{4}$$

where $TV_C m$, i, $\overline{TV_C}$, and $\delta_{m,i}$ are the i^{th}-pixel AWTS value in the m^{th} year (m = 10), time-averaged value, and standard deviation along a given AWTS over 10 years, respectively. $TV_C$is categorized in the same way as SV_C into three different groups, namely $0 < TV_C \leq 1$, $1 < TV_C \leq 2$, and $TV_C > 2$. Lower values can be regarded as reflecting the stable characteristics of AWTS over the time period.

(2) TV_F, the frequency of the temporal variation for AWTS, reflects the number of AWTS across the three TV_C classifications occurring repeatedly over ten years. $TV_F$is formulated simply as follows:

$$TV_F = \frac{TV_{C,P}}{\sum_{P=1}^{3} TV_{C,P}} \tag{5}$$

where P = 1, 2, 3. $TV_{C,P}$is the number of TV_C in each classification group ($TV_{C,1}$, $TV_{C,2}$, and $TV_{C,3}$) across the same pixel across 10 years, namely, $0 < TV_{C,1} \leq 1$, $1 < TV_{C,2} \leq 2$, and $TV_{C,3} > 2$. TV_F ranges from 0–10. The greater the frequency of low changes is, the greater the stability over time is.

(3) TV_R, the Pearson's correlation coefficient of AWTS, is used as a similarity measure for remote sensing time series (Lhermitte et al., 2011). Here, TV_R is formulated simply as follows:

$$TV_R = \frac{1}{j-1} \sum_{s=1}^{j} \left(\frac{V_{j,m} - \overline{V_{j,m}}}{\delta_{j,m}} \right) \left(\frac{V_{j,m+1} - \overline{V_{j,m+1}}}{\delta_{j,m+1}} \right) \tag{6}$$

where$V_{j,m}$ and $V_{j,m}$+1are a given AWTS of the j^{th} experimental region (j = 1–19) in the m^{th} and $(m + 1)^{th}$ years, $\overline{V_{j,m}}$ *and* $\overline{V_{j,m+1}}$are the average values of the two signals, and $\delta_{j,m}$ and $\delta_{j,m+1}$ are the standard deviations of the two signals. TV_Rranges from 0–1. The higher the TV_R value is, the more similar the signal curves are, and the better the stability of the stress signal is.

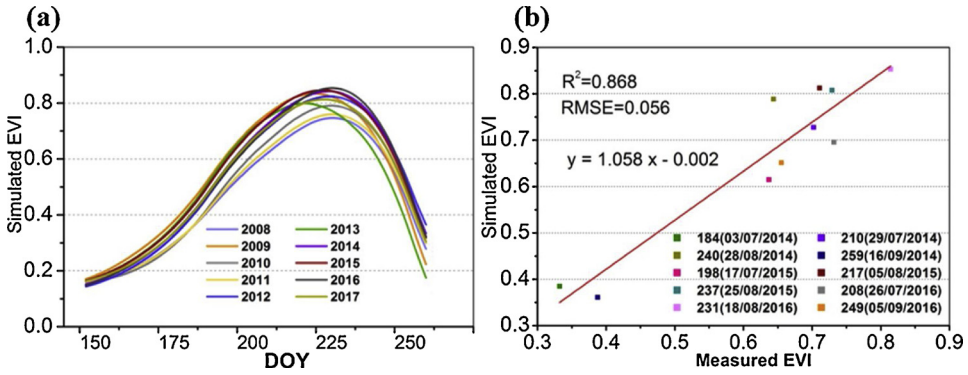

Fig. 3. EVI of healthy rice: (a) simulated EVI based on WOFOST and PROSAIL models over 10 years; (b) comparison of simulated EVI and measured EVI.

4. Results

4.1. Calculation of area wavelet transform stress signal (AWTS)

Using the WOFOST and PROSAIL models, the EVI of healthy rice (i.e., the potential or optimal productivity level) over 10 years was simulated. The input parameter values for the two models were set (Tables S4 and S5), and the same meteorological conditions and crop parameters in a given year prevailed throughout the area, while there were some differences in the meteorological conditions from year to year (Table S3). Therefore, each EVI simulates the growth curve of healthy rice in a given year (Fig. 3). As Fig. 3 details, the EVI initially increased and then gradually decreased. The EVI time series for healthy rice revealed the rice's inherent growth trend without stress. In addition, a comparison between the simulated EVI and measured EVI was made. As Fig. 3(b) shows, the R^2 of the simulated EVI versus the measured EVI was 0.87, which confirms the credibility of the simulation results.

Using the simulated EVI and EVI values for rice growth at the 19 sites, the AWTS was calculated on the basis of Fig. 2(c). The distribution of the area-averaged AWTS for every site from 2008–2017 are shown in Fig. 4. As this figure shows, most of the sites had AWTS values from 5 to 15 during that 10-yr period, and some of the abnormal values were found to be relatively high for some of the sites. Spatially, relatively higher values of area-averaged AWTS occurred at sites S4, S5, and S8. Lower area-averaged AWTS occurred at the sixteen other sites.

4.2. Spatio-temporal stability analysis of area wavelet transform stress signal (AWTS)

4.2.1. Spatial analysis of AWTS

Using Eq. (3), the SV_C of AWTS at each site was calculated. The annual cycle of the SV_C of AWTS from 2008–2017 is shown in Fig. 5.

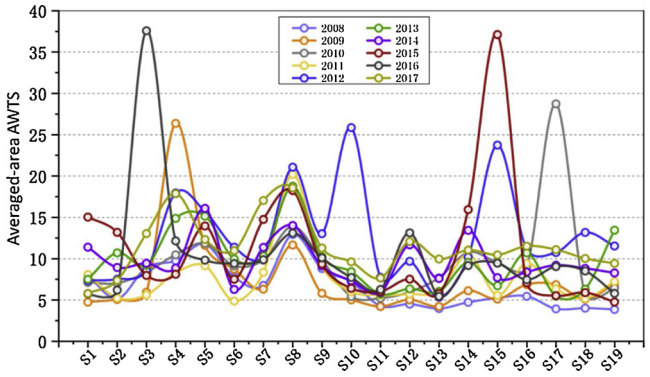

Fig. 4. Variation of area-averaged AWTS for 19 experimental sites over 10 years.

The spatial variation of the annual SV_C of AWTS was similar in every year. This figure clearly shows that the variability of SV_C was spatially and annually small. In addition, low values of the SV_C of AWTS (< 1) occurred over the 10 years and maintained a stable distribution for each experimental site. Fig. 6 shows the annual SV_C of AWTS by area (%) for each variation classification, with the SV_C of AWTS concentrated between 0 and 1 for most of the study area. Lower SV_C values (≤ 1) were relatively widespread throughout the study area, ranging from 70% to 95%. The maximum value of the SV_C area percentage occurred in 2016, while the minimum occurred in 2013. The second highest value of the SV_C coverage area was between 1 and 2. The SV_C coverage area varied from 5% to 25%. It should be noted that the area percentage variation of greater SV_C values (> 2) was less than 5%.

Based on the above analysis results, the area where the SV_C was concentrated between 0 and 1 was wide (greater than 70%), whereas the area where the SV_C exceeded 2 was small (less than 5%). This suggests that greater homogeneity existed in the AWTS output and resulted in uniform change in AWTS in the study area. When crops are stressed by heavy metals, AWTS exhibits spatial stability over 10 years.

4.2.2. Temporal analysis of AWTS

Fig. 7 illustrates the temporal variation of AWTS, including the mean value and standard value of AWTS over 10 years (Fig. 7(d) and (e)). The mean value of AWTS over the 10 years ranged mostly from 5 to 45, and the standard deviation of AWTS over the same time ranged mostly from 2 to 18. The spatial distribution and its statistical features were evaluated and compared for the three different variation classifications (Fig. 7(a), (b) and (c)). The TV_C of AWTS was concentrated between 0 and 1for each site. In general, lower TV_C values (≤ 1) were associated with larger frequency values, while values in the middle range ($1 < TV_C \leq 2$) and higher range ($TV_C > 2$) over the 10 years were associated with lower frequency values. To calculate the frequency value of TV_C over the 10 years (i.e., TV_F), ten different frequencies from 0 to 9 years (9-yr) were classified. Fig. 8 shows the area percentage (%) of the ten different frequencies for the three TV_C variation classification ranges. The relatively higher values ($TV_C > 2$) were limited to 1-yr; midrange values ($1 < TV_C \leq 2$) mostly remained connected with the time from 1-yr to 4-yr, and lower values ($TV_C \leq 1$) were mainly concentrated in 6-yr, 7-yr, 8-yr, and 9-yr with approximately 95% of the total area percentage. In short, the lower the value of TV_C is, the higher the value of TV_F is.

It is important to understand whether it is effective to derive a heavy metal stress signal for rice using WT. A comparison of the Pearson's correlation coefficient values for AWTS in the adjacent two years between Before-WT and After-WT was also conducted. As Table 1 shows, most of the Pearson's correlation coefficients of AWTS in the adjacent two years were higher than for the before-WT stress signal.

Based on the above analysis results, over ten years, the TV_C of AWTS in the range of 0–1 occurred frequently (more than 60% of the time), while the TV_C of AWTS exceeding 2 seldom happened. The Pearson

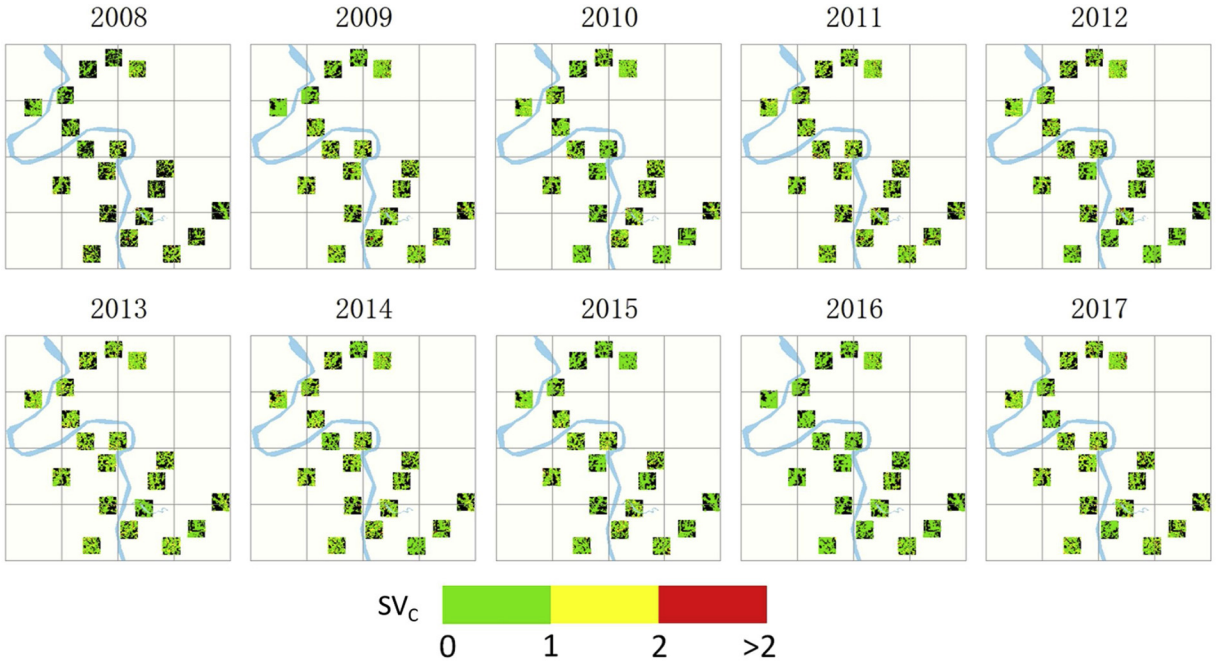

Fig. 5. Spatial variation of the coefficients of spatial variation (SV_c) over 10 years.

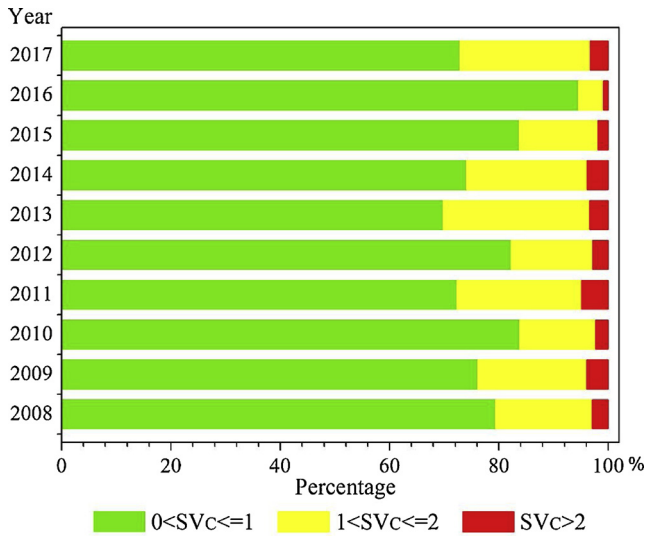

Fig. 6. Area percentage of the coefficients of spatial variation (SV_c) in each classification over 10 years.

correlation coefficient of AWTS over two consecutive years was usually greater than 0.5. This suggests that heavy-metal-induced stress in rice exhibits stable variability over a 10-yr time period.

5. Discussion

A small number of studies have attempted to apply NDVI or EVI to detect crop stress under saline conditions (Lobell et al., 2007, 2010; Platonov et al., 2013; Wu et al., 2014; Scudiero et al., 2014, 2016). Here, we demonstrated the use of EVI curves across all growth stages of a plant, instead of a single growth stage, to characterize persistent stress signal characteristics (Wang et al., 2015). Our study showed that heavy metal pollution in crops results in persistent and stable characteristics over space and time. An area wavelet transform stress signal (AWTS) could prove meaningful and effective as an indicator for crop stress monitoring and environmental assessment. Satisfactory performance was obtained, which can be attributed to two factors. First, the EVI of healthy rice, simulated using the WOFOST and PROSAIL models, reflects the rice growing at its potential productivity level, while the difference between simulated EVI values and the EVI values of rice growing in real agricultural ecosystems reflects the original stress signal, thereby isolating the effects of differences in environmental factors from year to year on the crop stress signal. Second, the original stress signal was decomposed into a detailed component and an approximation component using WT, and the approximation component was not affected by the "noise" introduced by the abrupt crop stress. This uncertainty has been shown to be much smaller when using the approximation component series, which behaves as a smoothing procedure and eliminates anomaly variations in the signal under certain scales (Martinez and Amparo Gilabert, 2009; Liu et al., 2011a, 2011b). That is to say, WT was implemented to decompose the original stress signal in order to isolate the effects of Cd stress from other confounding factors (de Beurs and Henebry, 2005; Scudiero et al., 2014; Tian et al., 2017).

Although we obtained better performance using our approach, errors in AWTS can be introduced in the following ways. (i) The PROSAIL and WOFOST models, which were coupled to simulate the EVI of healthy rice because of potential bias associated with the input parameters, such as LAI and the chlorophyll content. (ii) Reconstruction of the stressed rice EVI time series can introduce error as a result of the algorithm used to combine data from Landsat and MODIS and the VI time series fitting methods. (iii) Fallow crops in some years can result in an overestimation of AWTS. In this study, this occurred at site S4 in 2009, S10 in 2012, S15 in 2015, S3 in 2016, and S17 in 2017. We focused on a method for extracting the stress signal of rice under stable stress (i.e., Cd stress). Although the Cd concentration in the soil can affect changes in the crop stress signal, this relationship is difficult to quantify. Further work will be required to establish a model to detect the heavy metal stress levels of crops using a soil-plant system and to use this model to describe the occurrence of paddy soils contaminated with heavy metals.

6. Conclusion

This study established as method for deriving the Cd stress signal in rice and examined the spatio-temporal stability of Cd stress in rice in a

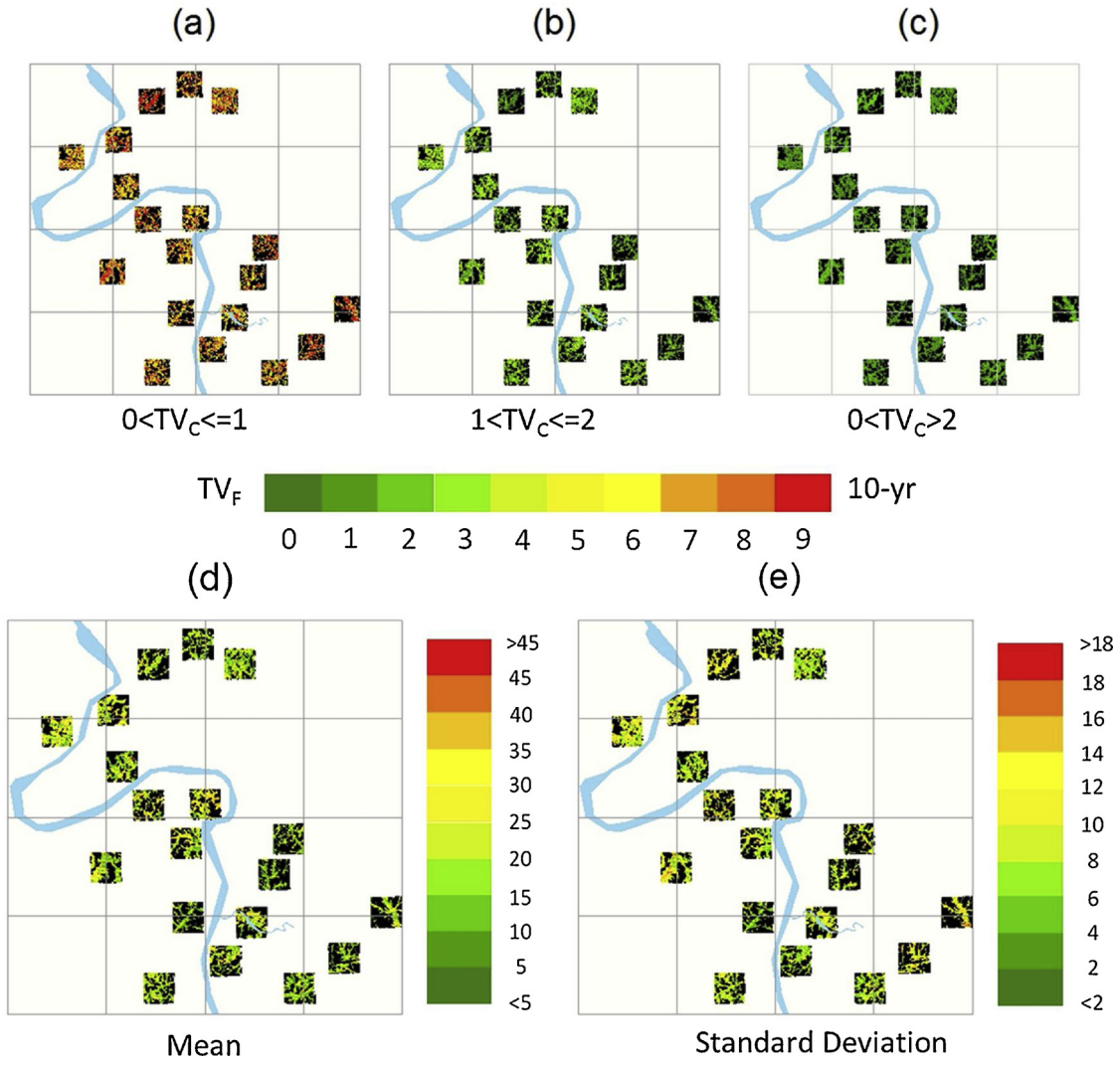

Fig. 7. Temporal variation of AWTS over 10 years: (a) the frequency value of lower values ($0 < TV_C \leq 1$); (b) the frequency value of midrange values ($1 < TV_C \leq 2$); (c) the frequency value of high values ($TV_C > 2$); (d) the mean value of AWTS ; (e)standard value of AWTS.

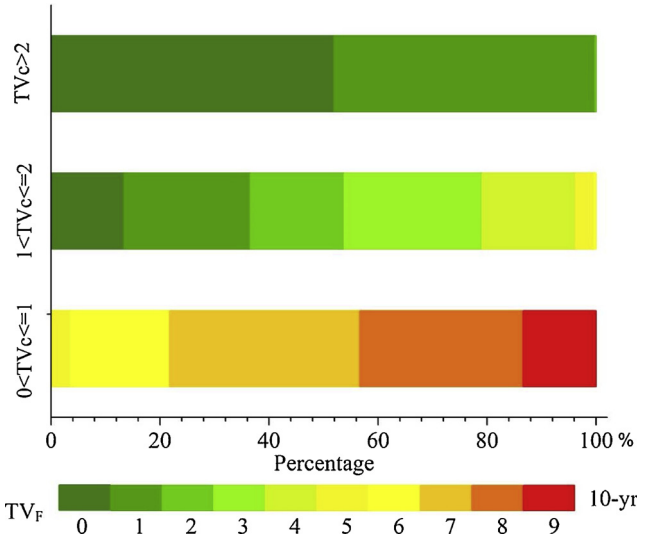

Fig. 8. Area percentage of the coefficients of temporal variation (TV_C) in each classification range over 10 years.

large study area in China over a period of 10 years. The coupling of the PROSAIL and WOFOST models was found to be an effective method of simulating the EVI of healthy rice in all the growth stages. MODIS and Landsat data corresponding to the rice growing seasons over a period of 10 years were combined to determine the EVI of rice under stress. A wavelet transform was used to derive the signal features of rice under stable stress by differentiating it from the stress signal of rice under abrupt stress. The area of the fifth low frequency signal (i.e., AWTS) can be used to quantify the features of rice under stable stress in all the growth stages. In addition, four key parameters of AWTS, namely the spatial variation coefficient (SV_C), the temporal variation coefficient (TV_C), the frequency of TV_C (TV_F), and TV_R can be used to characterize the spatial-temporal variation of rice under Cd stress. The SV_C and TV_C of AWTS were concentrated between 0 and 1 in the study area over the 10-yr period, regardless of the site and across different years, indicating the low spatio-temporal variability and stability of Cd-induced stress in rice over space and time. In addition, lower TV_C values were found to occur more often over the study period. The adjacent two years of AWTS values had greater Pearson correlation coefficients and exhibited a pattern consistent with those over the study period. The key parameters described above can effectively capture the spatio-temporal variation of rice under stable stress.

Thus, a wavelet transform can detect the stable stress signal of a crop by differentiating it from abnormal or abrupt stress signals. The

Table 1
Pearson's correlation coefficient of stress signal in the adjacent two years between Before-WT and After-WT.

	2008-2009	2009-2010	2010-2011	2011-2012	2012-2013	2013-2014	2014-2015	2015-2016	2016-2017
Before-WT	0.55	0.25	0.34	0.34	0.38	0.50	0.33	0.01	0.42
After-WT	0.73	0.77	0.65	0.37	0.79	0.50	0.77	0.10	0.79

physical models used, in combination with long-time-series remote sensing data, proved to be very promising in quantifying and understanding crop stress status in response to various environmental stressors and even potentially in response to climate change.

Acknowledgments

This research was financially supported by the National Natural Science Foundation of China (No. 41601473 and No. 41371407), the Fundamental Research Funds for the Central Universities (No. 2652017116 and No. 2652018080) and the China Scholarship Council and co-funded by the Faculty of Geo-Information Science and Earth Observation (ITC), University of Twente, the Netherlands.

References

Bradley, B.A., Jacob, R.W., Hermance, J.F., Mustard, J.F., 2007. A curve fitting procedure to derive inter-annual phenologies from time series of noisy satellite NDVI data. Remote Sens. Environ. 106 (2), 137–145.
Campos, A.N., Bella, C.M.D., 2012. Multi-temporal analysis of remotely sensed information using wavelets. J. Geogr. Inf. Syst. 4, 383–391.
Ceccato, P., Flasse, S., Tarantola, S., Jacquemoud, S., Gregoire, J.M., 2001. Detecting vegetation leaf water content using reflectance in the optical domain. Remote Sens. Environ. 77 (1), 22–33.
Chen, D., Guo, H., Li, R., Li, L., Pan, G., Chang, A., Joseph, S., 2016. Low uptake affinity cultivars with biochar to tackle Cd-tainted rice - a field study over four rice seasons in hunan. China. Sci. Total Environ. 541, 1489–1498.
de Beurs, K.M., Henebry, G.M., 2005. A statistical framework for the analysis of long image time series. Int. J. Remote Sens. 26 (8), 1551–1573.
Dhlamini, Z., Spillane, C., Moss, J.P., Ruane, J., Urquia, N., Sonnion, A., 2005. Status of Research and Application of Crop Biotechnologies in Developing Countries. Food and Agriculture Oganization of the United Nations Natural Resources Management and Environment Department, Rome, Italy.
Erasmi, S., Propastin, P., Kappas, M., Panferov, O., 2009. Spatial patterns of NDVI variation over indonesia and their relationship to ENSO warm events during the period 1982-2006. J. Clim. 22 (24), 6612–6623.
Feret, J.B., Francois, C., Asner, G.P., Gitelson, A.A., Martin, R.E., Bidel, L.P.R., Ustin, S.L., le Maire, G., Jacquemoud, S., 2008. PROSPECT-4 and 5: advances in the leaf optical properties model separating photosynthetic pigments. Remote Sens. Environ. 112 (6), 3030–3043.
Gao, F., Masek, J., Schwaller, M., Hall, F., 2006. On the blending of the landsat and MODIS surface reflectance: predicting daily landsat surface reflectance. ITGRS. 44 (8), 2207–2218.
Gao, F., Hilker, T., Zhu, X., Anderson, M.C., Masek, J.G., Wang, P., Yang, Y., 2015. Fusing landsat and MODIS data for vegetation monitoring. IEEE Geosci. Remote Sens. Mag. 3 (3), 47–60.
Hird, J.N., McDermid, G.J., 2009. Noise reduction of NDVI time series: an empirical comparison of selected techniques. Remote Sens. Environ. 113 (1), 248–258.
Hosgood, B., Jacquemoud, S., Andreoli, G., Verdebout, J., Pedrini, G., Schmuck, G., 1994. Leaf Optical Properties Experiment 93 (lopex93). Joint Research Centre / Institute for Remote Sensing Applications.
Huang, Z., Liu, X., Jin, M., Ding, C., Jiang, J., Wu, L., 2016. Deriving the characteristic scale for effectively monitoring heavy metal stress in rice by assimilation of GF-1 data with the WOFOST model. Sensors 16 (3).
Huete, A., Didan, K., Miura, T., Rodriguez, E.P., Gao, X., Ferreira, L.G., 2002. Overview of the radiometric and biophysical performance of the MODIS vegetation indices. Remote Sens. Environ. 83 (1-2), 195–213.
Jacquemoud, S., Verhoef, W., Baret, F., Bacour, C., Zarco-Tejada, P.J., Asner, G.P., Francois, C., Ustin, S.L., 2009. PROSPECT plus SAIL models: a review of use for vegetation characterization. Remote Sens. Environ. 113, 56–66.
Jin, M., Liu, X., Wu, L., Liu, M., 2015. An improved assimilation method with stress factors incorporated in the WOFOST model for the efficient assessment of heavy metal stress levels in rice. IJAEO 41, 118–129.
Jonsson, P., Eklundh, L., 2002. Seasonality extraction by function fitting to time-series of satellite sensor data. ITGRS 40 (8), 1824–1832.
Jonsson, P., Eklundh, L., 2004. TIMESAT - a program for analyzing time-series of satellite sensor data. Comput Geosci. 30 (8), 833–845.
Lei, M., Tie, B.Q., Song, Z.G., Liao, B.H., Lepo, J.E., Huang, Y.Z., 2015. Heavy metal pollution and potential health risk assessment of white rice around mine areas in Hunan Province. China. Food Secur. 7 (1), 45–54.
Levitt, J., 1980. Responses of plants to environmental stresses. Academic Press. 1 (5), 3642–3645.
Lhermitte, S., Verbesselt, J., Verstraeten, W.W., Coppin, P., 2011. A comparison of time series similarity measures for classification and change detection of ecosystem dynamics. Remote Sens. Environ. 115 (12), 3129–3152.
Li, Z.T., Kafatos, M., 2000. Interannual variability of vegetation in the United States and its relation to El Nino/Southern oscillation. Remote Sens. Environ. 71 (3), 239–247.
Lichtenthaler, H.K., 1998. The stress concept in plants: an introduction. Ann. N.Y. Acad. Sci. 851, 187–198.
Liu, J., Wang, L., Ma, L., Wu, W., Liu, Y., Sun, Y., 2004. A loss estimation method of monitoring and estimating the yield loss of wheat by drought in dry farming areas in northwest of China. Sci Agric Sin. 37 (2), 201–207.
Liu, M., Liu, X., Li, M., Fang, M., Chi, W., 2010. Neural-network model for estimating leaf chlorophyll concentration in rice under stress from heavy metals using four spectral indices. Biosyst. Eng. 106 (3), 223–233.
Liu, M., Liu, X., Ding, W., Wu, L., 2011a. Monitoring stress levels on rice with heavy metal pollution from hyperspectral reflectance data using wavelet-fractal analysis. IJAEO 13 (2), 246–255.
Liu, M., Liu, X., Wu, L., Duan, L., Zhong, B., 2011b. Wavelet-based detection of crop zinc stress assessment using hyperspectral reflectance. Comput. Geosci. 37 (9), 1254–1263.
Liu, F., Liu, X., Wu, L., Xu, Z., Gong, L., 2016a. Optimizing the temporal scale in the assimilation of remote sensing and WOFOST model for dynamically monitoring heavy metal stress in rice. IEEE J-STARS 9 (4), 1685–1695.
Liu, M., Liu, X., Liu, M., Liu, F., Jin, M., Wu, L., 2016b. Root mass ratio: index derived by assimilation of synthetic aperture radar and the improved world food study model for heavy metal stress monitoring in rice. J. Appl. Remote Sens. 10, 26–38.
Liu, M., Liu, X., Zhang, B., Ding, C., 2016c. Regional heavy metal pollution in crops by integrating physiological function variability with spatio-temporal stability using multi-temporal thermal remote sensing. Int. J. Appl. Earth Observ. Geoinform. 51, 91–102.
Liu, H., Zhang, K., Chai, L., Yang, Z., Yang, W., Liao, Q., Li, H., Liu, Y., 2017. A comparative evaluation of different sediment quality guidelines for metal and metalloid pollution in the Xingjian River, Hunan, China. Arch. Environ. Contam. Toxicol. 73 (4), 593–606.
Liu, M., Wang, T., Skidmore, A.K., Liu, X., 2018a. Heavy metal-induced stress in rice crops detected using multi-temporal Sentinel-2 satellite images. Sci. Total Environ 637–638, 18–29.
Liu, T., Liu, X., Liu, M., Wu, L., 2018b. Evaluating heavy metal stress levels in rice based on remote sensing phenology. Sensors 18 (3).
Lobell, D.B., Ortiz-Monasterio, J.I., Gurrola, F.C., Valenzuela, L., 2007. Identification of saline soils with multiyear remote sensing of crop yields. Soil Sci. Soc. Am. J. 71 (3), 777–783.
Lobell, D.B., Lesch, S.M., Corwin, D.L., Ulmer, M.G., Anderson, K.A., Potts, D.J., Doolittle, J.A., Matos, M.R., Baltes, M.J., 2010. Regional-scale assessment of soil salinity in the Red River Valley using multi-year MODIS EVI and NDVI. J. Environ. Qual. 39 (1), 35–41.
Martinez, B., Amparo Gilabert, M., 2009. Vegetation dynamics from NDVI time series analysis using the wavelet transform. Remote Sens. Environ. 113 (9), 1823–1842.
Montieth, J.L., 1996. The quest for balance in modeling. Agron. J. 88 (5), 695–697.
Nagajyoti, P.C., Lee, K.D., Sreekanth, T.V.M., 2010. Heavy metals, occurrence and toxicity for plants: a review. Environ. Chem. Lett. 8, 199–216.
Paliwal, A., Laborte, A., Nelson, A., Singh, R.K., 2018. Salinity stress detection in rice crops using time series MODIS VI data. Int. J. Remote Sens. 0, 1–17.
Percival, D.B., Walden, A.T., 2000. Wavelet Methods for Time Series Analysis. Cambridge University Press, pp. 594.
Piao, Y., Yan, B., Guo, S., Guan, Y., Li, J., Cai, D., 2012. Change detection of MODIS time series using a wavelet transform. Int. Conf. Syst. Inform. 2093–2097.
Platonov, A., Noble, A., Kuziev, R., 2013. Soil Salinity Mapping Using Multi-Temporal Satellite Images In Agricultural Fields of Syrdarya Province of Uzbekistan. Developments in Soil Salinity Assessment and Reclamation, pp. 87–89.
Ren, H., Zhuang, D., Singh, A., Pan, J., Qiu, D., Shi, R., 2009. Estimation of As and Cu contamination in agricultural soils around a mining Area by reflectance spectroscopy: a case study. Pedosphere 19 (6), 719–726.
Sakamoto, T., Yokozawa, M., Toritani, H., Shibayama, M., Ishitsuka, N., Ohno, H., 2005. A crop phenology detection method using time-series MODIS data. Remote Sens. Environ. 96 (3-4), 366–374.
Scudiero, E., Teatini, P., Corwin, D.L., Ferro, N.D., Simonetti, G., Morari, F., 2014. Spatiotemporal response of maize yield to edaphic and meteorological conditions in a saline farmland. Agron. J. 106 (6), 2163–2174.
Scudiero, E., Skaggs, T.H., Corwin, D.L., 2015. Regional-scale soil salinity assessment using Landsat ETM + canopy reflectance. Remote Sens.Environ. 169, 335–343.
Scudiero, E., Skaggs, T.H., Corwin, D.L., 2016. Comparative regional-scale soil salinity assessment with near-ground apparent electrical conductivity and remote sensing canopy reflectance. Ecol. Indic. 70, 276–284.

Srivastava, V., Sarkar, A., Singh, S., Singh, P., Araujo, A.A., Singh, R.P., 2017. Agroecological responses of heavy metal pollution with special emphasis on soil health and plant performances. Front. Environ. Sci. 52, 296–665X.
Tateishi, R., Ebata, M., 2004. Analysis of phenological change patterns using 1982-2000 advanced very High Resolution radiometer (AVHRR) data. Int. J. Remote Sens. 25 (12), 2287–2300.
Tian, L., Liu, X., Zhang, B., Liu, M., Wu, L., 2017. Extraction of rice heavy metal stress signal features based on long time series leaf area index data using ensemble empirical mode decomposition. Int. J. Environ Res. Public Health 14 (9).
Van Laake, P.E., Sanchez-Azofeifa, G.A., 2005. Mapping PAR using MODIS atmosphere products. Remote Sens. Environ. 94 (4), 554–563.
Wang, J., Price, K.P., Rich, P.M., 2001. Spatial patterns of NDVI in response to precipitation and temperature in the central Great plains. Int. J. Remote Sens. 22 (18), 3827–3844.
Wang, W., Yao, X., Tian, Y., Liu, X., Ni, J., Cao, W., Zhu, Y., 2012. Common spectral bands and optimum vegetation indices for monitoring leaf nitrogen accumulation in rice and wheat. J. Integr. Agric. 11 (12), 2001–2012.
Wang, J., Wang, T., Shi, T., Wu, G., Skidmore, A.K., 2015. A wavelet-based area parameter for indirectly estimating copper concentration in carex leaves from canopy reflectance. Remote Sens. 7 (11), 15340–15360.
Wang, F., Gao, J., Zha, Y., 2018. Hyperspectral sensing of heavy metals in soil and vegetation: feasibility and challenges. ISPRS J. Photogramm, Remote Sens. 136, 73–84.
Whitney, K., Scudiero, E., El-Askary, H.M., Skaggs, T.H., Allali, M., Corwin, D.L., 2018. Validating the use of MODIS time series for salinity assessment over agricultural soils in California, USA. Ecol. Indic. 93, 889–898.
Wu, L., Liu, X., Zhou, B., Liu, C., Li, L., 2012. Simulation of vegetation indices optimizing under retrieval of vegetation biochemical parameters based on PROSPECT + SAIL model. J. Appl. Ecol. 23 (12), 3250–3256.
Wu, L., Liu, X., Wang, P., Zhou, B., Liu, M., Li, X., 2013. The assimilation of spectral sensing and the WOFOST model for the dynamic simulation of cadmium accumulation in rice tissues. Int. J. Appl. Earth. Obs. 25 (1), 66–75.
Wu, W., Al-Shafie, W.M., Mhaimeed, A.S., Ziadat, F., Nangia, V., Payne, W.B., 2014. Soil salinity mapping by multiscale remote sensing in Mesopotamia, Iraq. IEEE J. Sel. Top. Appl. 7 (11), 4442–4452.
Zhou, G., Liu, X., Zhao, S., Liu, M., Wu, L., 2017. Estimating FAPAR of rice growth period using radiation transfer model coupled with the WOFOST model for analyzing heavy metal stress. Remote Sensing. 9 (5), 1–15.
Zhu, X., Chen, J., Gao, F., Chen, X., Masek, J.G., 2010. An enhanced spatial and temporal adaptive reflectance fusion model for complex heterogeneous regions. Remote Sens. Environ. 114 (11), 2610–2623.